Suspended Planar-Array Chips for Molecular Multiplexing at the Microscale

*Núria Torras, Juan Pablo Agusil, Patricia Vázquez, Marta Duch, Alberto M. Hernández-Pinto, Josep Samitier, Enrique J. de la Rosa, Jaume Esteve, Teresa Suárez, Lluïsa Pérez-García, and José A. Plaza**

Advances in biomolecular studies benefit enormously from the miniaturization of biological assays.[1,2] The identification, quantification, and determination of biochemical and physiological changes in small volumes[3] has been revolutionized by the use of planar arrays (PA).[4,5] PAs consist of a collection of multiple independent and ordered sensing features on a single device, allowing parallel assays. Progress towards size-reduction was continued by the emergence of suspended arrays (SA) of particles, whose advantages come from their fluid-phase kinetics, faster detection, and sample reduction.[1,6,7] However, they lose the critical advantage posed by the PA chips regarding the parallel assays using a single device.[1,2] In SA technologies, the tracking of individual assays[6] is guaranteed by subpopulations of particles each bearing a different molecular probe on their surfaces (array element), whereas each subpopulation is identified by a unique attribute (code).[6,7] Therefore, in recent years considerable effort has been focused on developing novel fabrication methods to encode microparticles.[8–12] Considering that particle size remains a critical property for many biological applications,[13–15] there is a continuous need to miniaturize monodisperse particles for further sample reduction and higher throughput.[3,9,16] One promising alternative is to achieve multiplexed biomolecular probes in a single suspended particle (i.e., patchy particles).[17,18] However, these particles are strongly limited by the impossibility of identifying each probe by its *x*-*y* position, their large volume compared with that of living cells,[19,20] and/or difficult multimaterial synthesis and chemical functionalization due to the necessary restrictive orthogonal-chemistry, which must allow different types of compatible chemical reactions to occur without interference on the same particle.[12,18,21]

Here, we introduce suspended planar-array (SPA) chips (**Figure 1**a) whose in-situ capabilities with a spatial molecular-probe arrangement combine the advantages of both SA and PA. This novel technology opens the way towards the multiplexed detection of intracellular biological parameters using a single device in dramatically reduced volumes, such as a living HeLa cell.

Silicon technologies based on photolithographic processes, such as those used for chip manufacturing, offer superb capabilities to produce complex 3D structures.[22] Thus, to produce SPA we developed a fabrication process (Figure 1b and S1) that started with the growth of a 1 µm thick SiO_2 layer as the chip-material on a silicon wafer. This material was selected due to its high transmission of light in the visible region of the spectrum, thus obtaining transparent chips. A subsequent photolithographic step followed by a dry etching process allowed the parallel arrangement, batch fabrication, and high miniaturization of the chips. We fixed the dimensions of the chips to $(3 \times 3 \times 1)$ µm^3 anticipating their use inside living cells, as the volume of the chips (9 µm^3) represents only ca. 0.35% of the total volume of a typical HeLa cell.[23,24] In addition, chips with similar dimensions have been shown to be easily internalized

Dr. N. Torras, M. Duch, Prof. J. Esteve, Dr. J. A. Plaza
Instituto de Microelectrónica de Barcelona
IMB-CNM (CSIC)
C/ dels Til·lers, Campus UAB
Cerdanyola del Vallès
Barcelona 08193, Spain
E-mail: joseantonio.plaza@imb-cnm.csic.es

Dr. J. P. Agusil,[+] Prof. J. Samitier
Nanobioengineering Group
Institute for Bioengineering of Catalonia (IBEC)
C/ Baldiri i Reixac 15–21
Barcelona 08028, Spain

Dr. P. Vázquez, Dr. A. M. Hernández-Pinto,
Dr. E. J. de la Rosa, Dr. T. Suárez
Centro de Investigaciones Biológicas, CIB (CSIC)
C/ Ramiro de Maeztu 9
Madrid 28040, Spain

Prof. J. Samitier
Department d'Electrònica
Universitat de Barcelona
C/ Martí i Franquès 1
Barcelona 08028, Spain

Prof. J. Samitier
Centro de Investigación Biomédica en Red en Bioingeniería
Biomateriales y Nanomedicina (CIBER-BBN)
C/ María de Luna 11, Edificio CEEI
Zaragoza 50018, Spain

Dr. L. Pérez-García[++]
Departament de Farmacologia i Química Terapèutica
Institut de Nanociència i Nanotecnologia (IN2UB)
Universitat de Barcelona
Av. Joan XXIII s/n, Barcelona 08028, Spain

[+]Present address: Instituto de Microelectrónica de Barcelona, IMB-CNM (CSIC), C/ dels Til·lers, Campus UAB, Cerdanyola del Vallès, Barcelona, 08193, Spain

[++]Present address: School of Pharmacy, The University of Nottingham, University Park, Nottingham, NG7 2RD, England, UK

DOI: 10.1002/adma.201504164

ADVANCED MATERIALS
www.advmat.de

www.MaterialsViews.com

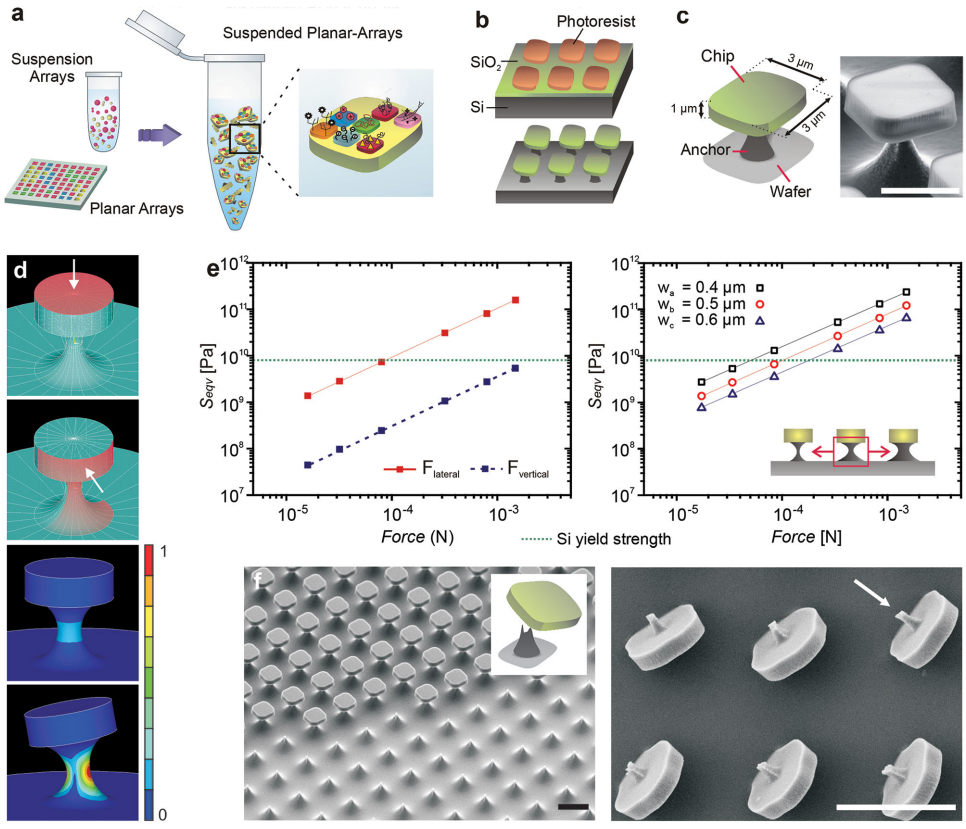

Figure 1. The suspended planar-arrays chips concept, fabrication and release. a) Conceptual description of the SPA chips arisen from the combination of PA and SA. b) Schematic representation of the fabrication of the SPA chips at two stages. Top: a SiO_2 layer defines the thickness of the chips and a photolithographic step followed by SiO_2 etching process defines their shape and lateral dimensions. Bottom: nanomachining of the mechanical anchors. c) Fabricated chips at the wafer stage. Left: Schematic view of the main parts. Right: A detailed SEM image. Scale bar = 3 µm. d) FEM of the mechanical performance of the anchored chips versus applied forces. Top: Model and applied loads. White arrows indicate vertical and lateral forces. Bottom: Simulated Von Misses stresses, normalized to the highest value. e) Simulated results of the maximum equivalent Von Misses stress, S_{eqv}, on the silicon anchor: Left: for vertical and lateral forces. Right: for lateral forces as a function of the width of the anchor. Horizontal green dashed line indicates silicon yield strength limit. f) SEM images. Left: wafer with partially released chips. Right: detail of released chips showing the fracture of the anchor (white arrow). Scale bars = 5 µm.

inside living HeLa cells and to affect neither the cell viability nor the cell division.[25] Using this highly-reproducible technology we produced 2.7×10^6 chips cm^{-2}. Chip-release from the wafer was a main issue as it must respect the eventual printed molecule pattern. We developed a release method based on controlled nanofracture. Consequently, anchors with non-uniform cross-sections were nanomachined underneath the chips (Figure 1c) by time-controlled anisotropic silicon etching. The anchor dimensions were optimized with the finite element method (FEM) (Figure 1d) to bear an initial molecular-printing process and on-demand fracture to collect the chips. The mechanical stresses concentrate on the narrowest part of the silicon anchor for vertical and lateral forces. Lateral rather than vertical forces induce larger stresses and the maximum stress-concentration was dependent on the width of the narrowest part of the anchor (Figure 1e). Accordingly, the width of the narrowest part of the anchor was designed to be ca. 450 nm, expecting a fracture with a lateral force of above 85 µN or a vertical force higher than 3.3×10^3 µN. Our experimental tests confirmed the fracture on the predicted anchor region without damaging the chip (Figure 1f).

Soft lithographic techniques allow the direct placement of molecules adsorbed on a stamp on a desired substrate. Among these techniques, polymer pen lithography (PPL),[26] uses sharp elastomeric pens to print localized and spatially distributed features, offering the possibility to create 2D grids of motifs.[27] This patterning approach combines the large-area printing capabilities of microcontact printing with the potential nanometric resolution of Dip-Pen nanolithography.[28] We used PPL to pattern molecules directly on the area-restricted surfaces of the anchored chips (**Figure 2**a). This parallel printing method uses the same chemistry and immobilization protocol for each molecular probe overcoming the required orthogonal chemistry. Briefly, the top surface of the anchored chips was selectively modified with an epoxy-silane coupling agent.[29,30] Then, a polydimethylsiloxane (PDMS) PPL stamp (Figure S2 and S3), whose spatial distribution of elastomeric pens matched that of the anchored chips was used to print an identical and precise molecular pattern on every single anchored chip. A glass slide attached to the back of the stamp prevented any contraction.[31] The stamp was loaded onto our PPL apparatus where the printing force and the precise alignment between the stamp and the substrate were monitored

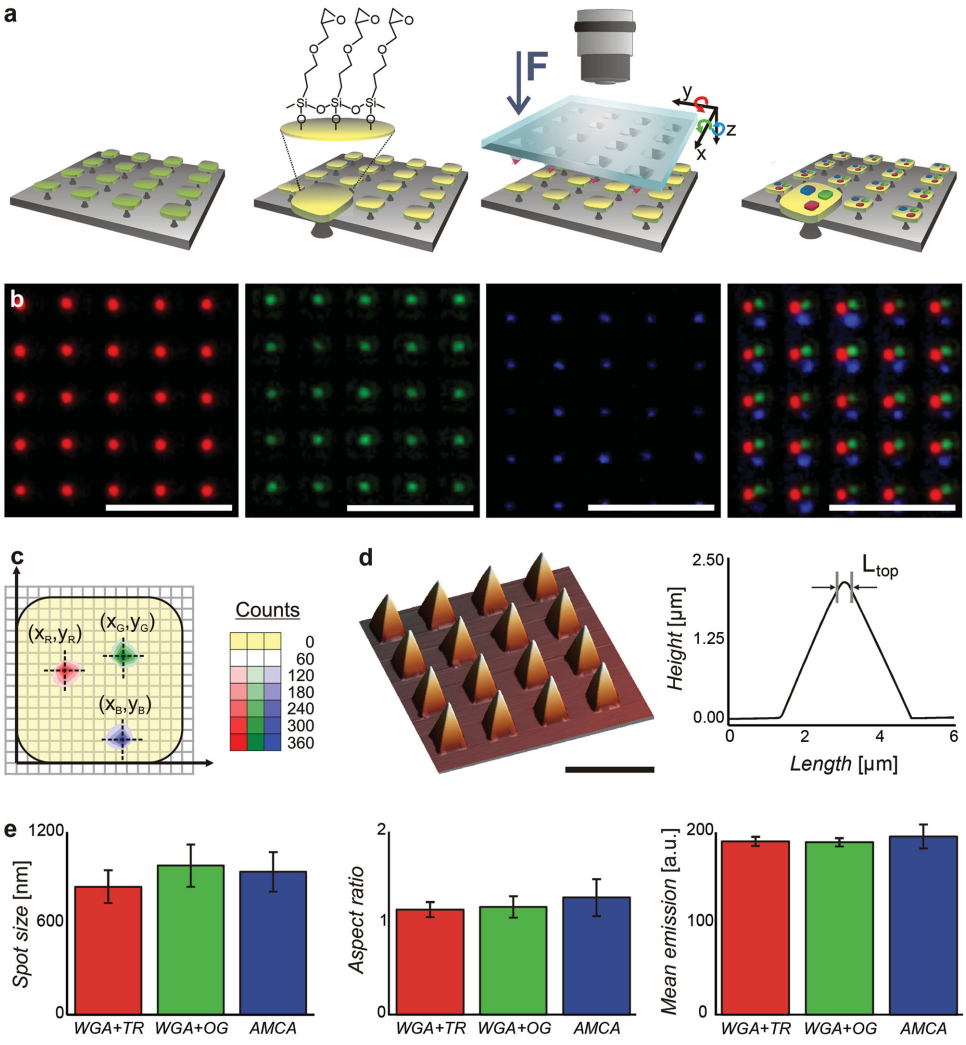

Figure 2. Multiplexed polymer pen lithography on 3D anchored chips. a) Scheme of the molecular printing on three-dimensional chips. Left: anchored chips at wafer level. Center-left: functionalization of the SiO_2 top surface with an epoxy-terminated SAM. Center-right: parallel molecular print by a PPL stamp. Right: multiple printings generate multiplexed array on each single chip. b) Fluorescence microscopy images of multiplexed anchored chips. From left to right: Texas Red WGA (red), Oregon Green 488 WGA (green), AMCA rabbit anti-Goat IgG (H+L) (blue) and the overlay. Scale bars = 15 µm. c) Heat map presenting the counts for the localization (x_i, y_i), i = R(red), G(green), B(Blue), of the three printed molecules on the spatial reference system of each single chip. d) The pens at the PDMS PPL stamp. Left: 3D topographical AFM image of a 4 × 4 array of pens. Right: AFM profile of a single polymer pen before compression. Scale bar = 10 µm. e) Graphical representation of the printed spots for each molecule. From left to right: spot size, aspect ratio, and mean fluorescent emission. Data are presented as the mean ± standard deviation. c) and e) n = 784.

(Figure S4), assuring that all the pens were localized and exerted the same force on each anchored chip.

To demonstrate the multiplexing capability, we initially printed three individually-labelled proteins on top of the anchored chips. Specifically, three areas of a stamp were independently inked with Texas Red wheat germ agglutinin (WGA), Oregon Green 488 WGA, and AMCA (7-amino-4-methylcoumarin-3-acetic acid) rabbit anti-Goat IgG (H+L), and consecutively printed (Figure S5, Movie S8). The three fluorophores had different absorption and emission maxima, λ_{Abs} = (596, 501, 344) nm and λ_{Emi} = (615, 526, 446) nm, respectively. Fluorescence characterization showed a 2D spatial arrangement of printed molecules (Figure 2b-c). We decided to print spots of Ø ~ 1 µm to allow a feasible inspection on fluorescence and confocal laser scanning microscopes (CLSM). Mainly, two parameters contribute to the size of the printed spots, the apex diameter of the PDMS pyramidal pens before compression, L_{top}, and the applied printing force, F,[32] which deforms the pens during writing. By applying an experimental total F of 480 mN ± 2 mN (0.17 µN per pen), with an average pen L_{top} of 212 nm ± 23 nm (Figure 2d), we predicted a spot diameter of 742 nm ± 62 nm. This value agrees with the experimentally obtained spot mean value of 962 nm ± 207 nm. The printed spots showed similar aspect ratios and fluorescence emissions across the fluorescent channels (Figure 2e). These results demonstrate a theoretical density < 1 spot µm^{-2}.

To release the printed chips from the wafer, we developed a simple but highly effective peel-off method (**Figure 3**a). A drop of an aqueous mounting medium was first placed directly on top of the anchored chips. A subsequent manual force was

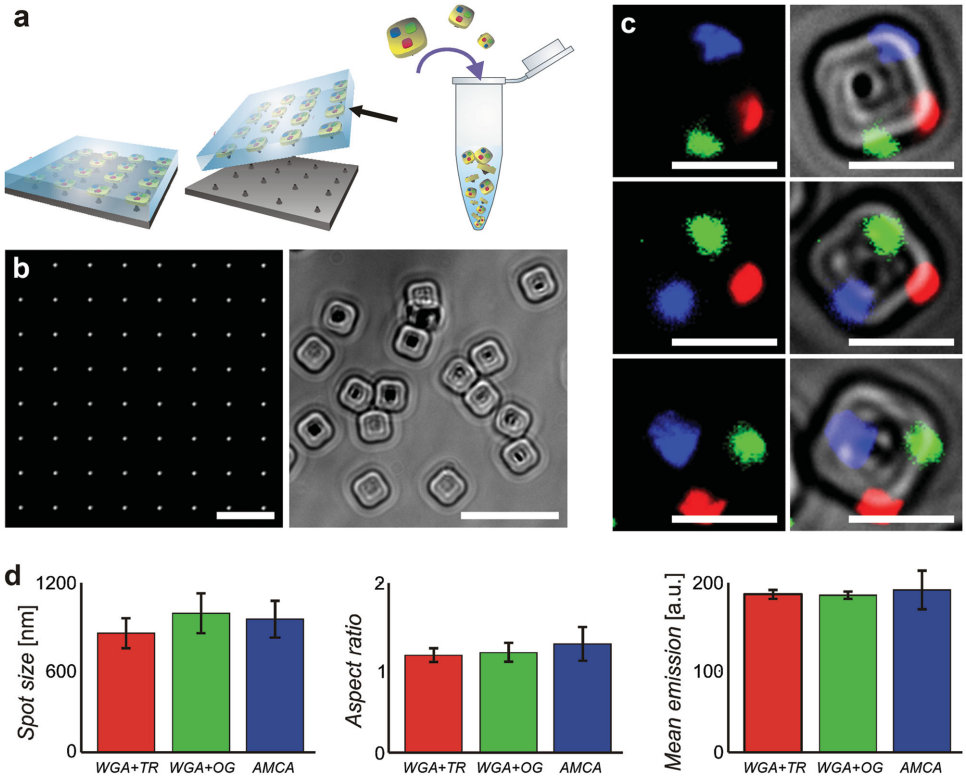

Figure 3. Released multiplexed chips. a) Scheme of the developed peel-off method and collection. From left to right: a solidified drop of liquid mounting medium covers the wafer, the polymeric solid layer is peeled-off liberating the printed chips which are embedded in the layer; the membrane is lastly dissolved. b) Optical images after the peel-off process. Left: remaining anchors on the wafer. Right: released chips. All the chips are detached and removed from the wafer. Scale bars = 10 μm. c) Fluorescence microscopy images of three representative multiplexed collected chips. Left panels: overlaid images of Texas Red WGA (red), Oregon Green 488 WGA (green) and AMCA rabbit anti-Goat IgG (H+L) (blue) spots on top of each chip. Right panels: An overlay of the previous images with the transmission channel (visible). Scale bar = 3 μm. d) Graphical representation of the printed spots for each molecule. From left to right: spot size, aspect ratio, and mean fluorescent emission. Data are presented as the mean ± standard deviation (n = 25).

used to peel the solidified, flexible membrane encircling the chips. The chips were collected by centrifugation after dissolving the water-soluble membrane (Figure 3b). Liberated chips were structurally intact as predicted by mechanical simulations (Movie S9), and fluorescence microscopy showed that the printed molecular-spots remained on the chips (Figure 3c) showing spot size, aspect ratios and fluorescence emissions (Figure 3d) as those before being released. Furthermore, an antibody sandwich assay, using a primary goat anti-WGA and a secondary AMCA rabbit anti-Goat IgG (H+L), confirmed the integrity of the printed proteins (Figure S6).

In order to demonstrate the major achievement of these devices, we decided to detect, as a proof of concept, externally induced pH changes towards living HeLa cells. Three commercially available probes were multiplexed on a new set of previously aminofunctionalized SPA chips: two pH-sensitive fluorescent dyes (Oregon Green 488 and pHrodo Red), for a ratiometric detection, and one control dye (Alexa 647) (**Figure 4**a). The SPA chips were successful internalized by lipofection into HeLa cells, as previously demonstrated.[23] After lipofection, the cells were stained with MitoTracker Red and examined via CLSM to confirm the internalization of multifunctionalized SPA chips (Figure 4b). In order to test whether the chips affected cell viability, in vivo DiOC6 staining was used to analyze mitochondrial membrane potential, finding no differences between cells with or without internalized chips (Figure 4c) in agreement with previous results.[23,25]

After internalization, CLSM images showed that the three printed fluorescent probes remained clearly visible inside the cells (Figure 4d and S7), even after 72 h of culture. Next, the external pH of the medium was changed from physiological pH 7.4 to pH 5. Nigericin was added to force the cell-membrane exchange of H^+ ions, therefore altering the intracellular pH and, consequently, changing the fluorescence emitted by the two pH-sensitive multiplexed dyes on the internalized SPA chips (Figure 4d). The fluorescence intensity of the pHrodo Red and Oregon Green 488 spots, after normalization to the Alexa 647 intensity, increased and decreased, respectively. Finally, the ability of this new multiplexed device allowed us a ratiometric detection (Oregon Green 488/pHrodo Red fluorescence ratio) that certainly detected the pH change, even when the SPA chips inside HeLa cells appeared tilted (Figure S7).

We have proved SPA chips as a new concept for molecular probes at microscale allowing 2D arranged multiplexed assays in a single device. An extraordinary high density spotting in a single SPA chip is anticipated, as PPL can reach a sub-100 nm printing resolution.[28] Our technology allows the batch fabrication of SPA with high potential anisotropy-attributes,[33] together with the

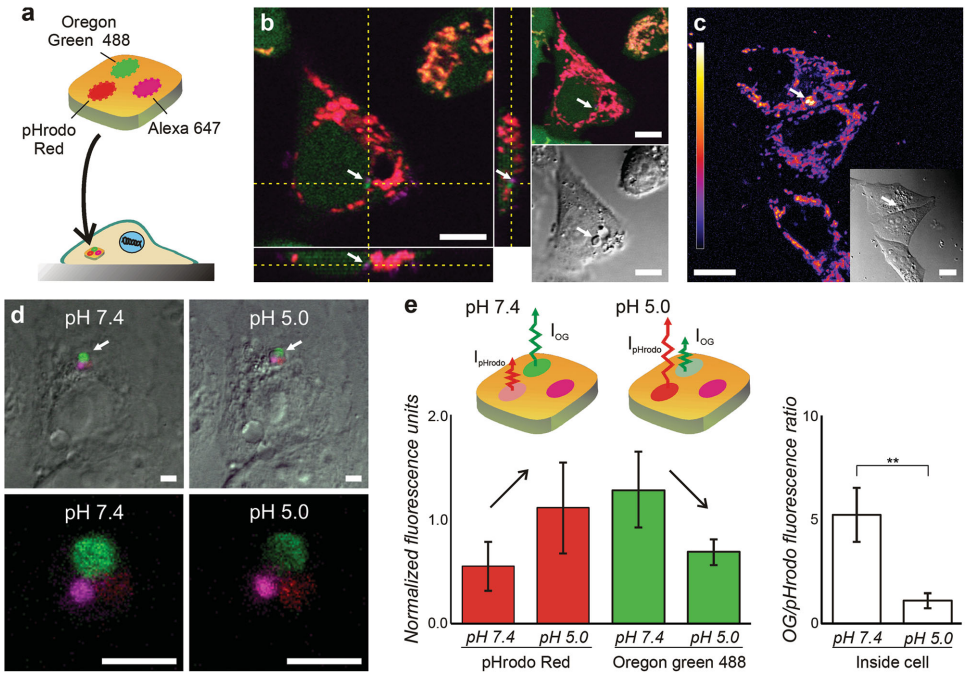

Figure 4. SPA chips inside HeLa living cells. a) Schematic representation of the SPA chips with the three fluorescent probes to detect pH changes inside living cells. b) In vivo CLSM image showing a HeLa cell loaded with MitoTracker Red (mitochondria) and an internalized SPA chip. The orthogonal projection of CLSM images demonstrates that the chip is inside the cell. The right panels show the overlay image of the confocal stacks and an optical Nomarski image. Scale bars = 10 μm. c) In vivo CLSM image of HeLa cells stained with the mitochondrial potential-dependent probe DiOC6 and an internalized SPA chip. The pseudo-colored pixel-mean-intensity image shows that HeLa cells with and without an internalized SPA chip exhibit identical DiOC6 labelling. Inset: an optical Nomarski image showing the localization of the chip. Scale bars = 10 μm. d) SPA chips inside HeLa cells respond to pH changes. The same HeLa cells in culture media at pH 7.4 (left) and after switching the culture medium to pH 5 (right) in the presence of nigericin, to equilibrate external and internal pHs. In the top panels we show the overlay image of a confocal stack and an optical Nomarski image. White arrows point the SPA chip. The bottom panels present the overlay images of the same chips. Scale bars = 3 μm. e) Measurement of the fluorescence intensities of pHrodo Red and Oregon Green 488 at different pH values. The top panel represents the SPA chips and the predicted fluorescence changes at different pHs. Below, the graph on the left, represents the experimental quantification of Oregon Green 488 and pHrodo Red fluorescence intensities of different SPA chips inside HeLa cells ($n > 6$), normalized by the intensity of the Alexa 647 (magenta) for each SPA chip, at pH 7.4 and pH 5. The graph on the right shows the ratio of the fluorescence intensities Oregon Green 488 and pHrodo Red (OG/pHrodo) at pH 7.4 and pH 5. Data are presented as the mean ± standard deviation of at least five experiments. Statistical comparison pH 5 vs pH 7.4: **$p<0.01$ (unpaired t-test).

dramatic miniaturization of the PA chips offering in situ, high-throughput and new potential applications. We demonstrated the first PA chip inside a living cell and the potential use of molecular printing techniques for intracellular applications. Living-arrays[3,16] have been developed to observe from the exterior the response of living cells to external stimuli. SPA chips allow single-cell intracellular analysis. Emerging intracellular arrays would allow the identification of physicochemical intracellular parameters related to genetic determinants of diseases, cellular-function modulators or dynamic responses of the cell to its local environment, allowing researchers to attain their goal of analyzing multiple bioparameters inside single living cells.[2,13,16]

Experimental Section

Materials: All reagents and materials were purchased from different providers and used without further purification. The complete protocols are detailed in the Supporting Information.

Fabrication: Details of the SPA fabrication process along with the numerical simulations and optimization by the FEM, the PPL patterning protocol, stamp and apparatus, together with cell culture conditions are fully described in the Supporting Information.

Characterization: All characterization tools and protocols used in this work are presented in the Supporting Information.

Supporting Information

Supporting Information is available from the Wiley Online Library or from the author.

Acknowledgements

This work was supported by the EU ERDF (FEDER) funds and the Spanish Government grants TEC2011-29140-C03-01/02 and TEC2014-51940-C2-1/2. PV was supported by a JAE-DOC contract (FSE funding). The authors also thank the cleanroom staff of IMB-CNM for fabrication of the chips and the confocal microscopy service of the CIB.

Received: August 26, 2015
Revised: September 23, 2015
Published online: December 9, 2015

[1] S. F. Kingsmore, *Nat. Rev. Drug Discov.* **2006**, *5*, 310.
[2] A. Q. Emili, G. Cagney, *Nat. Biotechnol.* **2000**, *18*, 393.
[3] S. Sauer, B. M. H. Lange, J. Gobom, L. Nyarsik, H. Seitz, H. Lehrach, *Nat. Rev. Genet.* **2005**, *6*, 465.
[4] G. MacBeath, S. L. Schreiber, *Science* **2000**, *289*, 1760.
[5] L. A. Liotta, V. Espina, A. I. Mehta, V. Calvert, K. Rosenblatt, D. Geho, P. J. Munson, L. Young, J. Wulfkuhle, E. F. Petricoin, *Cancer Cell* **2003**, *3*, 317.
[6] K. Braeckmans, S. C. De Smedt, *Nat. Mater.* **2010**, *9*, 697.
[7] J. P. Nolan, L. A. Sklar, *TRENDS Biotechnol.* **2002**, *20*, 9.
[8] K. Braeckmans, S. C. De Smedt, M. Leblans, R. Pauwels, J. Demeester, *Nat. Rev. Drug Discov.* **2002**, *1*, 447.
[9] D. Dendukuri, D. C. Pregibon, J. Collins, T. A. Hatton, P. S. Doyle, *Nat. Mater.* **2006**, *5*, 365.
[10] D. C. Pregibon, M. Toner, P. S. Doyle, *Science* **2007**, *315*, 1393.
[11] H. Lee, J. Kim, H. Kim, J. Kim, S. Kwon, *Nat. Mater.* **2010**, *9*, 745.
[12] Y. Zhao, Y. Cheng, L. Shang, J. Wang, Z. Xie, Z. Gu, *Small* **2015**, *11*, 151.
[13] C. Schubert, *Nature* **2011**, *480*, 133.
[14] Q. F. Wills, K. J. Livak, A. J. Tipping, T. Enver, A. J. Goldson, D. W. Sexton, C. Holmes, *Nat. Biotechnol.* **2013**, *31*, 748.
[15] S. Bhaskar, K. M. Pollock, M. Yoshida, J. Lahann, *Small* **2010**, *6*, 404.
[16] M. L. Yarmush, K. R. King, *Annu. Rev. Biomed. Eng.* **2009**, *11*, 235.
[17] Z. Zhang, S. C. Glotzer, *Nano Lett.* **2004**, *4*, 1407.
[18] a) S. Rahmani, S. Saha, H. Durmaz, A. Donini, A. C. Misra, J. Yoon, J. Lahann, *Angew. Chemie* **2014**, *126*, 2364; b) *Angew. Chem. Int. Ed.* **2014**, *53*, 2332.
[19] K. Maeda, H. Onoe, M. Takinoue, S. Takeuchi, *Adv. Mater.* **2012**, *24*, 1340.
[20] J. Lee, P. W. Bisso, R. L. Srinivas, J. J. Kim, A. J. Swiston, P. S. Doyle, *Nat. Mater.* **2014**, *13*, 524.
[21] S. Jiang, Q. Chen, M. Tripathy, E. Luijten, K. S. Schweizer, S. Granick, *Adv. Mater.* **2010**, *22*, 1060.
[22] E. Fernandez-Rosas, R. Gómez, E. Ibañez, L. Barrios, M. Duch, J. Esteve, C. Nogués, J. A. Plaza, *Small* **2009**, *5*, 2433.
[23] R. Gómez-Martínez, A. M. Hernández-Pinto, M. Duch, P. Vázquez, K. Zinoviev, E. J. de la Rosa, J. Esteve, T. Suárez, J. A. Plaza, *Nat. Nanotechnol.* **2013**, *8*, 517.
[24] L. Zhao, C. D. Kroenke, J. Song, D. Piwnica-Worms, J. J. H. Ackerman, J. J. Neil, *NMR Biomed.* **2008**, *21*, 159.
[25] R. Gómez-Martínez, P. Vázquez, M. Duch, A. Muriano, D. Pinacho, N. Sanvicens, F. Sánchez-Baeza, P. Boya, E. J. de la Rosa, J. Esteve, T. Suárez, J. A. Plaza, *Small* **2010**, *6*, 499.
[26] F. Huo, Z. Zheng, G. Zheng, L. R. Giam, H. Zhang, C. A. Mirkin, *Science* **2008**, *321*, 1658.
[27] X. Liao, A. B. Braunschweig, C. A. Mirkin, *Nano Lett.* **2010**, *10*, 1335.
[28] A. B. Braunschweig, F. Huo, C. A. Mirkin, *Nat. Chem.* **2009**, *1*, 353.
[29] D. Fine, A. Grattoni, R. Goodall, S. S. Bansal, C. Chiappini, S. Hosali, A. L. van de Ven, S. Srinivasan, X. Liu, B. Godin, L. Brousseau, I. K. Yazdi, J. Fernandez-Moure, E. Tasciotti, H.-J. Wu, Y. Hu, S. Klemm, M. Ferrari, *Adv. Healthcare Mater.* **2013**, *2*, 632.
[30] R. Ganesan, K. Kratz, A. Lendlein, *J. Mater. Chem.* **2010**, *20*, 7322.
[31] D. J. Eichelsdoerfer, X. Liao, M. D. Cabezas, W. Morris, B. Radha, K. A. Brown, L. R. Giam, A. B. Braunschweig, C. A. Mirkin, *Nat. Protoc.* **2013**, *8*, 2548.
[32] X. Liao, A. B. Braunschweig, Z. Zheng, C. A. Mirkin, *Small* **2010**, *6*, 1082.
[33] S. C. Glotzer, M. J. Solomon, *Nat. Mater.* **2007**, *6*, 557.